Order parameter for the transition from strong to weak generalized synchrony from empirical mode decomposition analysis

Kaustubh Manchanda and Ramakrishna Ramaswamy
School of Physical Sciences, Jawaharlal Nehru University, New Delhi 110067, India
(Received 9 February 2011; published 7 June 2011)

We examine driven nonlinear dynamical systems that are known to be in a state of generalized synchronization with an external drive. The chaotic time series of the response system are subject to empirical mode decomposition analysis. The instantaneous intrinsic mode frequencies (and their variance) present in these signals provide suitable order parameters for detecting the transition between the regimes of strong and weak generalized synchrony. Application is made to a variety of chaotically driven flows as well as maps.

DOI: 10.1103/PhysRevE.83.066201 PACS number(s): 05.45.Ac, 05.45.Pq, 05.45.Xt

I. INTRODUCTION

The most general—and possibly the most ubiquitous—form of temporal correlation between systems is their generalized synchronization (GS) [1]. When one dynamical system is driven by another, if the response signal is *uniquely* dependent on the drive, then the two are said to be in generalized synchrony.

The simplest case, when the drive and response are both linear, can be completely analyzed, and a synchronization viewpoint has little additional insight to offer [2]. However, when either the drive and/or the response is chaotic, such a categorization appears to be useful. If the evolution equations of the drive and response are given by

$$\dot{\mathbf{u}} = F(\mathbf{u}), \tag{1}$$

$$\dot{\mathbf{x}} = G(\mathbf{x},\mathbf{u}), \tag{2}$$

respectively, then in GS there is a (possibly implicit) functional dependence of the response $\mathbf{x}$ on the drive $\mathbf{u}$, namely

$$\mathbf{x} = \Phi[\mathbf{u}]. \tag{3}$$

The function Φ need not be differentiable even if the vector fields of the drive and response, namely F and G, are continuous and smooth. This defines the states of strong and weak generalized synchrony [4]: When Φ is differentiable, the GS is strong, and, contrastingly, if it is not differentiable, it is termed weak GS. As was shown by Abarbanel *et al.* [3] either case of GS may be detected by constructing an auxiliary system, namely an identical copy of the response,

$$\dot{\mathbf{x}}' = G(\mathbf{x}',\mathbf{u}) \tag{4}$$

and observing the complete synchronization of $\mathbf{x}$ and $\mathbf{x}'$.

In the typical situation, as a coupling parameter is varied, there is a transition between strong and weak GS. Recent work [5–7] has shown that this transition can have different characteristics depending on the manner in which the parameter space is traversed. There are distinct "routes" from strong and weak GS, and these share similarities with the routes to chaos in nonlinear dynamical systems without driving, as well as to the routes to strange nonchaotic motion in quasiperiodically driven systems [8].

Along these routes, though, the transition from strong to weak generalized synchrony can be difficult to detect, and some earlier studies, notably by Pyragas [4] and Hunt, Ott, and Yorke [9], have addressed the issue of the strong $\rightarrow$ weak transition in different ways. The differentiability of the implicit function Φ can be quantified through the Hölder exponent [9,10]. Other methods have also been proposed for the detection of the nondifferentiability of the implicit function [11,12], particularly in the analysis of time-series data [13]. Some rigorous results on the continuity of the function Φ have been obtained by Afraimovich, Chazottes, and Cordonet [14], but these can be difficult to apply in the general case.

In the present work we show that the analytical signal analysis (ASA) [15], together with the empirical mode decomposition [16], offers an efficient tool for detection of the strong-to-weak GS transition. Measures based on the empirical mode frequencies and their variance provide an unambiguous signature of this transition and can be applied quite generally. Indeed, a recent study has shown the utility of the ASA methodology in a study of the transition to phase synchronization (PS) [17,18] that can be similarly difficult to detect. In recent years a very large number of applications of the ASA technique have established that this can be a reliable, and powerful method for examining complex temporal signals, with some advantages vis-à-vis traditional spectral tools such as the Fourier or wavelet transform [16].

The standard empirical mode decomposition and the ASA method is briefly discussed in the following section. In Sec. III, application is made to the analysis of continuous and discrete nonlinear dynamical systems displaying weak and strong generalized synchronization. The paper concludes with a discussion and summary in Sec. IV.

II. ANALYTICAL SIGNAL ANALYSIS AND EMPIRICAL MODE DECOMPOSITION

In order to be able to associate an amplitude and phase to an arbitrary complex aperiodic signal $x(t)$ it is necessary to construct an "analytical signal," $\psi(t)$ [15],

$$\psi(t) = x(t) + i\tilde{x}(t), \tag{5}$$

where

$$\tilde{x}(t) = \frac{1}{\pi}\mathrm{PV}\left[\int_{-\infty}^{\infty}\frac{x(t')}{t-t'}dt'\right] \tag{6}$$

is the Hilbert transform of x, with PV denoting the Cauchy principal value. This then makes it possible to define the amplitude of the signal as

$$A(t) = \sqrt{x(t)^2 + \tilde{x}(t)^2} \tag{7}$$

and the corresponding phase as

$$\phi(t) = \arctan[\tilde{x}(t)/x(t)]. \tag{8}$$

Although somewhat arbitrary, this method of assigning the amplitude and phase reduces to standard definitions for sinusoidal or periodic signals and if $x(t)$ is not periodic, then both the amplitude $A(t)$ and the instantaneous frequency $\omega(t) = \dot{\phi}(t)$ are not constant and the nature of their variation is related to the underlying dynamics.

The constructed analytical signal must satisfy two conditions, namely that it should have a well-defined center and that there should be a preferred direction of rotation for the instantaneous frequencies to be physically meaningful. A complex signal that does not possess such a proper structure of rotation needs to be decomposed into a sum of proper rotations via the empirical mode decomposition (EMD) method developed by Huang *et al.* [16].

This algorithm [16] is based on the assumption that the signal $s(t)$ has at least two extrema from which a characteristic time scale can be obtained. The innate oscillations that belong to different time scales can be individually extracted one mode at a time by using the envelope of the local maxima and minima. Identification of the intrinsic modes is done as follows: the local maximum and minimum of the signal are found and are connected by a cubic spline to form the upper envelope $cs_{\max}(t)$ and the lower envelope $cs_{\min}(t)$, respectively. Their mean,

$$m(t) = \tfrac{1}{2}[cs_{\max}(t) + cs_{\min}(t)], \tag{9}$$

is subtracted from the original signal $s(t)$ to yield $d(t)$

$$d(t) = s(t) - m(t). \tag{10}$$

If $d(t)$ is a proper rotation, it is an intrinsic mode. Else, a "sifting" procedure is employed, namely now one uses $d(t)$ as the signal to analyze. From $d(t) \longrightarrow d(t) - m(t)$, the upper and lower envelopes $[cs_{\max}(t), cs_{\min}(t)$, respectively] are formed, and the above procedure is carried out recursively until $d(t)$ has the structure of a proper rotation. This yields the first intrinsic mode function (IMF) $B_1(t) = d(t)$ that corresponds to the highest-frequency oscillations contained in the original signal since the envelopes are constructed using the extrema of the highest-frequency waves. After subtracting this shortest time-scale component from the original signal $s(t)$,

$$s(t) \longrightarrow s(t) - B_1(t), \tag{11}$$

this entire process is iterated to yield the second intrinsic mode $B_2(t)$. Subsequent iterations then give a sequence of modes that capture the different time scales, and each intrinsic mode is, by construction, a pure rotation in the complex plane with a meaningful instantaneous frequency. After extracting these modes, if the residual signal $s(t)$ is such that it has less than two local extrema, or its amplitude is negligible compared to the original signal, the process is terminated. This residual component, $\epsilon(t)$, has vanishingly small amplitude with at most quadratic dependence on time. Thus the original signal $s(t)$ is empirically decomposed into a set of modes

$$s(t) = \sum_{i=1}^{M} B_i(t) + \epsilon(t) = B_s(t) + \epsilon(t). \tag{12}$$

Given a mode $u_D(t)$ of the drive, and the corresponding mode of the response $x_R(t)$, a plausible functional relationship between them extends Eq. (3) as

$$x_R(t) = \Phi[u_D(t)]. \tag{13}$$

If $H[\cdot]$ is the Hilbert transform operator, with

$$H[u_D(t)] = \tilde{u}_D(t), \tag{14}$$

one can see that the differentiability properties of Φ are pertinent in relating the two Hilbert transforms since

$$\tilde{x}_R(t) = \tilde{u}_D(t)(\Phi' + \ldots). \tag{15}$$

Interpretation of the instantaneous modes in terms of physical properties has not been straightforward [16]. As shown by Lai and Ye [19] for periodic or quasiperiodic motion, the fundamental frequencies obtained in the analytical signal representation correspond approximately to those obtained in the Fourier transform, but when the motion is chaotic, the Fourier spectrum is broadband while the instantaneous frequencies obtained from analytical signal analysis remain localized. There is thus no simple correspondence between the two spectra. In a number of model examples, Lee *et al.* [20] have shown that the dominant empirical IMFs are the responses of the "slow–flow" modes of the dynamics. For complex signals coming from chaotic oscillators, the physical significance of the modes can be difficult to discern.

At the same time, measures derived from the EMD have been shown to provide suitable order parameters for detecting the onset of phase synchrony between two oscillators coupled unidirectionally [17,18]. Since the transition from strong GS to weak GS is a consequence of the loss of differentiability of the implicit functional relationship between response and drive, one may expect a signature of this change in dynamics to reflect in quantities that are derived from the EMD analysis. As we show in the next section, the mode frequencies and their variance provide suitable order parameters.

III. APPLICATIONS

Generalized synchrony is clearest in unidirectionally coupled systems, namely those with a skew-product structure, and when the drive and the response are both nonlinear, with at least one of them having chaotic dynamics [4–6]. In an earlier study, we have considered a simple harmonic drive with a quasiperiodic frequency [21]; in that case, the transition of interest is from quasiperiodic tori to strange nonchaotic attractors [8].

Our protocol in the present work is as follows. For a given value of the control parameter, we generate N trajectories of length T and extract the largest frequency modes [16] according to the procedure described above. Each of the IMFs is then subject to the analytical signal analysis via the Hilbert transform method described, and for each IMF, the phase and average instantaneous frequencies ν_i^k can be determined. The

subscript i labels the individual modes, and the superscript k, the different trajectories in the ensemble. By averaging over the ensemble, the mean mode frequency $\omega_i = \sum_{k=1}^{N} \nu_i^k / N$ and variance, $\sigma_i^2 = \omega_i^2 - \sum_{k=1}^{N} (\nu_i^k)^2$ at this value of the control parameter can be obtained.

We study the variation of ω_2, namely the frequency of the second mode in the present analysis. The first intrinsic mode of the response is dominated by the drive characteristics and thus a transition in the response dynamics on varying the coupling can be difficult to detect. The higher modes have instantaneous frequencies that are distinct from those of the drive and are well localized. Thus the second and higher modes appear to capture dynamical features that are present in the response signal and that are not simply a reflection of the drive. Numerical errors in the EMD algorithm increase as one goes to higher order [16] and therefore, although in principle any of the mode frequencies can be used to detect the transition, it is preferable to use ω_2 and its variance.

We make application to three systems below. For the signals studied here, the number of modes is typically less than 10.

A. Rössler-Lorenz Flow

The first example we consider has the chaotic Rössler oscillator [22] as a drive

$$\begin{aligned} \dot{u}_1 &= -\alpha(u_2 + u_3) \\ \dot{u}_2 &= \alpha(u_1 + a u_2) \\ \dot{u}_3 &= \alpha[b + u_3(u_1 - c)] \end{aligned} \tag{16}$$

and the Lorenz attractor [23] as response,

$$\begin{aligned} \dot{x}_1 &= 10(-x_1 + x_2) \\ \dot{x}_2 &= 28x_1 - x_2 - x_1 x_3 + k u_2 \\ \dot{x}_3 &= x_1 x_2 - 8x_3/3. \end{aligned} \tag{17}$$

The multiplier α is introduced in order to control the characteristic time scale of the drive and is here taken to be 6; the other parameters in the Rössler system are $a = b = 0.2$, and $c = 5.7$. Earlier work by Pyragas has suggested that there is a transition from weak to strong generalized synchrony in the range $20 \leqslant k \leqslant 50$, although GS itself occurs when $k > 6$ [4].

The dynamics of the Lorenz response Eq. (17) is subjected to EMD. In particular, we carry out the analysis on $s(t) = x_1(t)$ as shown in Fig. 1(a). The IMF analysis is presented in Fig. 2 for a fixed value of the coupling $k = 15$ when the GS is weak. The signal carries eight intrinsic modes that can be represented as proper rotations; the sum of these eight IMFs essentially reconstructs the original signal Fig. 3(a) with a negligible residue as can be seen in Fig. 3(b).

The functional relationship between the Hilbert transforms of the response and drive [cf. Eq. (15)] is shown in Fig. 4. For weak GS ($k = 15$), the fluctuations are significantly larger (indicative, we believe, of a nonsmooth Φ) in comparison to $k = 30$ that is strong GS. To locate the *transition* from weak to strong GS we examine ω_2 and its variance: There is a significant decrease in the variance at $k \approx 24$ [Fig. 5(b)], suggesting that there is a change in the functional relationship between the two quantities.

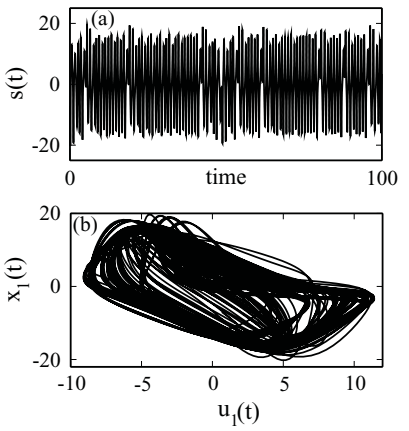

FIG. 1. (a) The signal $s(t)$ chosen for analysis is the variable $x_1(t)$ from the driven Lorenz oscillator, Eq. (17). (b) A plot of the response $x_1(t)$ as a function of the drive, $u_1(t)$, showing the complex functional dependence.

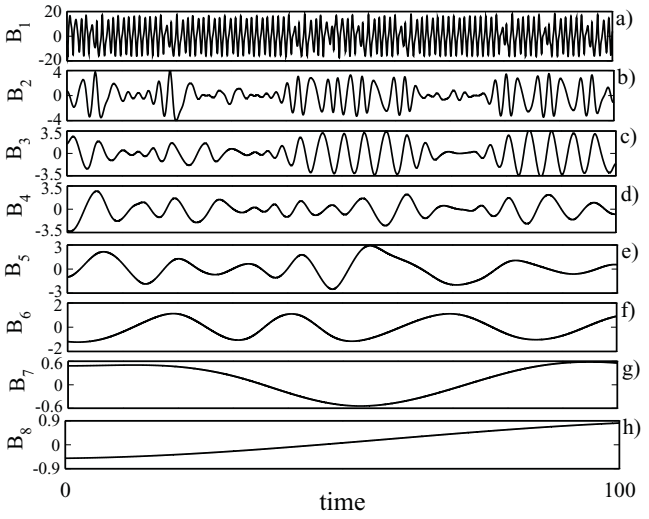

FIG. 2. The signal $s(t)$ shown in Fig. 1 yields the eight intrinsic modes, B_i, that are shown above. The coupling strength $k = 15$ falls within the regime of weak generalized synchrony.

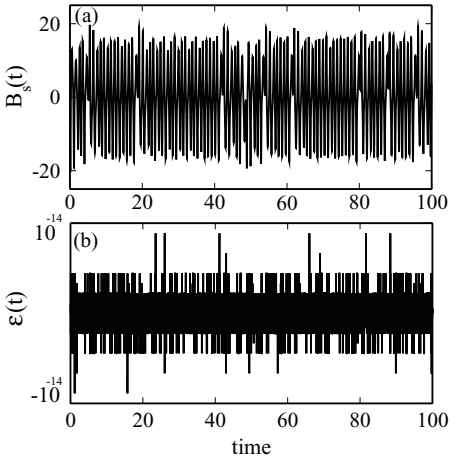

FIG. 3. (a) $B_s(t)$, the sum of the eight IMFs shown in Fig. 2 that are obtained from the signal $s(t)$. (b) The residual error $\epsilon(t)$.

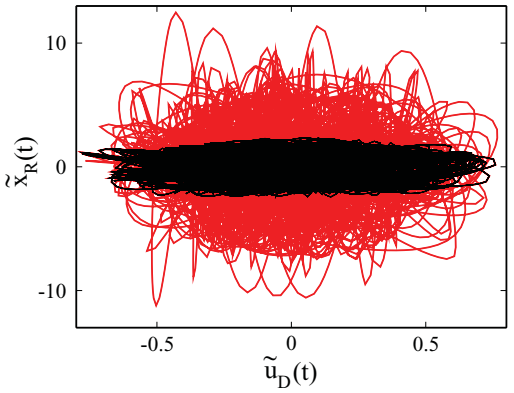

FIG. 4. (Color online) The Hilbert transform of the third mode of the response $\tilde{x_R}(t)$ as a function of the Hilbert transform of the corresponding mode of the drive, $\tilde{u_D}(t)$ [using Eq. (15)] in the strong ($k = 30$, black) and the weak (k =15, red/gray) GS regimes.

This correlates with the change in the dynamics from weak to strong GS: We verify this independently by computing the parameter sensitivity of the dynamics [24,25]. This quantity assesses the variability in the dynamical attractor when the system parameters are varied, and as can be seen in Fig. 6, the parameter sensitivity exponent begins to saturate around $k \approx$, 24 thus indicating the onset of strong GS. The order parameter used by Pyragas [4] is the mean thickness σ of the map Φ estimated from the Kaplan-Yorke dimension [26]. Evaluation of this latter quantity does not lead to a clear transition point in contrast to the present EMD analysis.

B. Baker-Logistic map

The second system we study is the chaotically driven logistic mapping [5],

$$x_{n+1} = \alpha(1 + \epsilon \cos 2\pi u_n)x_n(1 - x_n) \tag{18}$$

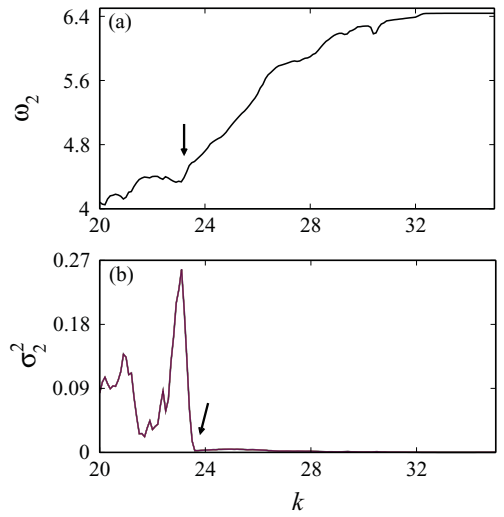

FIG. 5. (Color online) In the Rössler-Lorenz system, (a) the frequency ω_2 and (b) its variance σ_2^2 for the second mode as a function of k. The transition from weak to strong GS occurs at $k \approx 24$ when the variance decreases significantly.

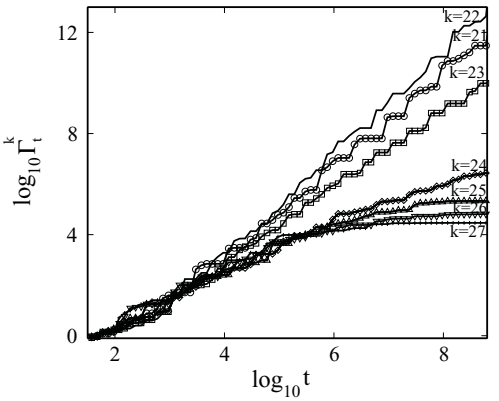

FIG. 6. Parameter sensitivity at different coupling strengths; the saturation of the curve for the coupling $k \approx 24$ indicates the onset of strong GS.

where $x \in [0, [1]$, $\alpha \geqslant 2$, and the drive u is provided by the generalized baker transformation [27],

$$u_{n+1} = \begin{cases} bu_n & v_n < a \\ b + (1-b)u_n & v_n \geqslant a \end{cases} \tag{19}$$

$$v_{n+1} = \begin{cases} v_n/a & v_n < a \\ (v_n - a)/(1-a) & v_n \geqslant a \end{cases} \tag{20}$$

with $a = b = 0.45$.

This dynamical system exhibits a number of scenarios [5] for the transition from strong to weak generalized synchrony that include fractalization, doubling collisions, and intermittency at different values of the parameters α and ϵ, and we examine each of these routes through the EMD.

Following the procedure outlined above, the time series of the response map is subject to IMF analysis, and the discrete modes are extracted. Figures 7(a) and 7(b) show the variation of the second mode frequency and its variance as a function of the parameter α for fixed $\epsilon = 0.03$. Both the frequency and the variance signal the weak-to-strong GS transition at $\alpha \approx 3.8325$

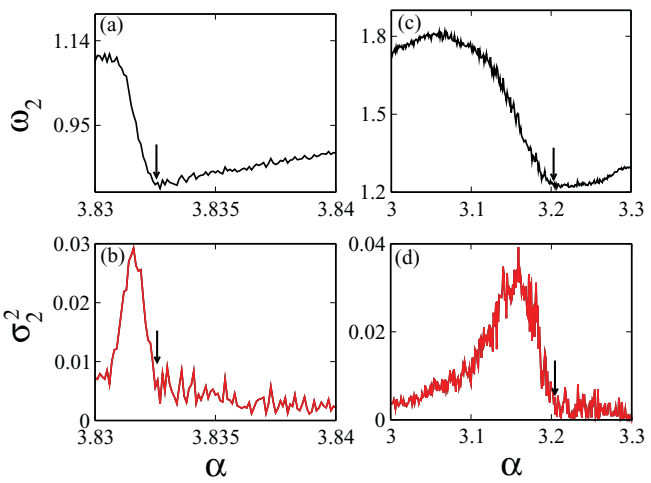

FIG. 7. (Color online) For the chaotically driven logistic map, (a) and (b) are the frequency ω_2 and variance σ_2^2 for the second mode as a function of α for $\epsilon = 0.03$. The same quantities at $\epsilon = 0.15$ are shown in (c) and (d). The transition from weak to strong GS occurs at $\alpha \approx 3.8325$ and $\alpha \approx 3.21$, respectively, in the two cases.

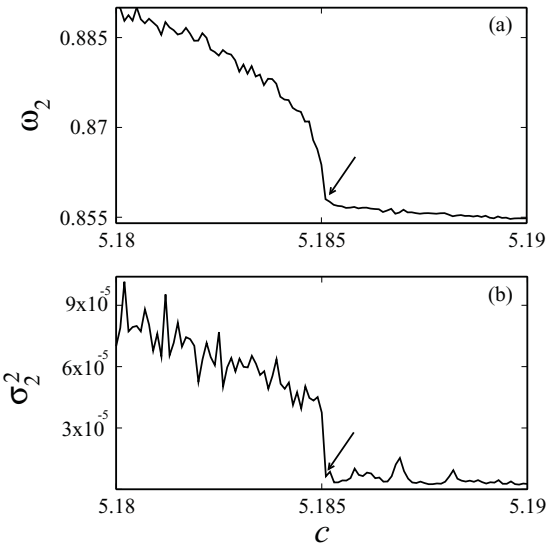

FIG. 8. Transition from weak to strong GS in the Rössler drive-Duffing response system. The frequency ω_2 (a) and (b) its variance σ_2^2 as a function of the parameter c for mode 2.

that occurs via the intermittency route [5]. A sharp change in these quantities is also observed when the transition occurs via a doubling collision at $\alpha \approx 3.21$ for $\epsilon = 0.15$, as shown in Figs. 7(c) and 7(d). The transition via fractalization, which is seen at $\epsilon = 0.2$ [5] remains elusive with the present approach: Neither the frequency nor the variance show any distinctive change beyond a possible inflection point at $\alpha \approx 2.6$ [5] (these results are not shown here).

C. The driven Duffing oscillator

The final application here is of a chaotically forced Duffing oscillator [6] given by the evolution equations

$$\begin{aligned} \dot{x}_1 &= x_2 \\ \dot{x}_2 &= -hx_2 - x_1^3 + [1 + A(\cos x_3 + a_r u_1)]x_1 \\ \dot{x}_3 &= 1. \end{aligned} \tag{21}$$

The total modulation in Eq. (21) is a superposition of two signals: a sinusoidal drive and $u_1(t)$ that we take here to be the output of the Rössler drive, Eq. (16) with $a = b = 0.2$, $\alpha = 1.49$. Recall that when the drive is also taken to be sinusoidal with an irrational frequency, then there can be transitions to strange nonchaotic attractors [28–30]. The coupling between drive and response is fixed with a_r at 0.125, $h = 0.2$, $A = 0.15$, and the Rössler oscillator parameter c is used as a control.

This system has been studied earlier studied by Singh *et al.* [6], who used the largest subsystem Lyapunov exponent to detect the transition from weak to strong GS. Using the response variable $x_1(t)$ for EMD analysis, we compute the intrinsic mode frequencies and variances which are shown in Figs. 8(a) and 8(b). A sharp change is clearly evident at the critical value $c \approx 5.185$, in agreement with earlier results.

We have verified that when the drive is more complex—for example, a chaotic Lorenz system—the above procedure is equally effective in detecting the transition from weak to strong GS (results not shown here).

IV. DISCUSSION AND SUMMARY

A host of recent applications, ranging from climate data [31,32] to biomedical signals [33,34], have shown that the empirical mode decomposition technique is a versatile and informative tool for the analysis of complex signals.

We have applied the EMD here for the detection of a somewhat subtle transition within the regime of generalized synchrony based on the observation that the fluctuation properties of the signals change across the transition. The substructure of GS can thus be explored by this method: The frequency and variance corresponding to the different intrinsic modes serve as good order parameters for detection of the transition from strong to weak GS. We have studied chaotically driven flows as well as maps that show this transition; the present analysis can detect the transition in each case, and the characteristic signature of the transition appears to depend on the particular "route" to weak GS [5].

EMD analysis complements earlier studies [4,9] that have used a variety of measures to detect the weak-to-strong GS transition. An order parameter that examines the degree of coherence between the two signals (as measured in the permutation entropy of each signal) has also been used [13], but this is sometimes insensitive to the transition to generalized synchrony itself.

The present method decomposes a given signal on the basis of local characteristic time scales *within* the data. This is suitable even when the data are nonstationary. The method is adaptive and therefore highly efficient to implement computationally. It can equally well be applied to time-series and to high dimensional systems and may thus be of practical use in examining experimental instances of generalized synchrony.

ACKNOWLEDGMENTS

We thank Awadhesh Prasad, Rajat Karnatak, and Shakir Bilal for valuable discussions. K.M. acknowledges support from the University Grants Commission.

[1] N. F. Rulkov, M. M. Sushchik, L. S. Tsimring, and H. D. I. Abarbanel, Phys. Rev. E **51**, 980 (1995).
[2] N. C. Bobillo-Ares and J. Fernández-Nuñez, Eur. J. Phys. **16**, 223 (1995).
[3] H. D. I. Abarbanel, N. F. Rulkov, and M. M. Sushchik, Phys. Rev. E **53**, 4528 (1996).
[4] K. Pyragas, Phys. Rev. E **54**, R4508 (1996).
[5] T. U. Singh, A. Nandi, and R. Ramaswamy, Phys. Rev. E **78**, 025205 (2008).
[6] T. U. Singh, H. H. Jafri, and R. Ramaswamy, Phys. Rev. E **81**, 016208 (2010).

[7] T. U. Singh and R. Ramaswamy, NDES2009: The 17th International IEEE Conference "Nonlinear Dynamics of Electronic Systems," Rapperswil, Switzerland, 21–24 June, 2009 (Unpublished).
[8] A. Prasad, S. S. Negi, and R. Ramaswamy, Int. J. Bifurcat. Chaos **11**, 291 (2001).
[9] B. R. Hunt, E. Ott, and J. A. Yorke, Phys. Rev. E **55**, 4029 (1997).
[10] L. Guo and Z. Xu, Chaos **18**, 033134 (2008).
[11] N. F. Rulkov and V. S. Afraimovich, Phys. Rev. E **67**, 066218 (2003).
[12] D. He, Z. Zheng, and L. Stone, Phys. Rev. E **67**, 026223 (2003).
[13] Z. Liu, Europhys. Lett. **68**, 19 (2004).
[14] V. Afraimovich, J. R. Chazottes, and A. Cordonet, Discrete Contin. Dyn. Syst., Ser. B **1**, 421 (2001).
[15] D. Gabor, J. Inst. Electr. Eng. (London) Part III **93**, 429 (1946).
[16] N. E. Huang, Z. Shen, S. R. Long, M. C. Wu, H. H. Shih, Q. Zheng, N. C. Yen, C. C. Tung, and H. H. Liu, Proc. R. Soc. London A **454**, 903 (1998).
[17] A. Goska and A. Krawiecki, Phys. Rev. E **74**, 046217 (2006).
[18] M. Chavez, C. Adam, V. Navarro, S. Boccaletti, and J. Martinerie, Chaos **15**, 023904 (2005).
[19] Y. C. Lai and N. Ye, Int. J. Bifurcat. Chaos **13**, 1383 (2003).
[20] Y. S. Lee, S. Tsakirtzis, A. F. Vakakis, L. A. Bergman, and D. M. McFarland, AIAA J. **47**, 2938 (2009).
[21] K. Gupta, A. Prasad, H. P. Singh, and R. Ramaswamy, Phys. Rev. E **77**, 046220 (2008).
[22] O. Rössler, Phys. Lett. A **57**, 397 (1976).
[23] E. N. Lorenz, J. Atmos. Sci. **20**, 130 (1963).
[24] T. Nishikawa and K. Kaneko, Phys. Rev. E **54**, 6114 (1996).
[25] A. Jalnine and S. Y. Kim, Phys. Rev. E **65**, 026210 (2002).
[26] J. L. Kaplan and J. A. Yorke, in *Functional Differential Equations and Approximation of Fixed Points*, Springer Lecture Notes in Mathematics, edited by H.-O. Peitgen and H.-O. Walther, Vol. 730 (Springer-Verlag, Berlin, 1979), p. 204.
[27] J. D. Farmer, E. Ott, and J. A. Yorke, Physica D **7**, 153 (1983).
[28] J. Heagy and W. L. Ditto, J. Nonlinear Sci. **1**, 423 (1991).
[29] A. Prasad, V. Mehra, and R. Ramaswamy, Phys. Rev. Lett. **79**, 4127 (1997).
[30] A. Venkatesan, M. Lakshmanan, A. Prasad, and R. Ramaswamy, Phys. Rev. E **61**, 3641 (2000).
[31] M. K. I. Molla, M. S. Rahman, A. Sumi, and P. Banik, Discrete Dyn. Nat. Soc. **2006**, 1 (2006).
[32] K. Coughlin and K. K. Tung, in *Hilbert-Huang Transform and Its Applications*, edited by N. E. Huang and S. S. P. Shen (World Scientific, Singapore, 2005), pp. 149–168.
[33] H. Liang, S. L. Bressler, R. Desimone, and P. Fries, Neurocomputing **65/66**, 801 (2005).
[34] R. B. Northrop, *Signals and Systems Analysis in Biomedical Engineering* (CRC Press LLC, Boca Raton, FL, 2003).